IEEE Access
Multidisciplinary : Rapid Review : Open Access Journal

Received 9 October 2025, accepted 9 November 2025, date of publication 12 November 2025, date of current version 18 November 2025.

Digital Object Identifier 10.1109/ACCESS.2025.3631840

RESEARCH ARTICLE

Design of a Deployable Offset Mesh Reflector Antenna Utilizing a Deployable Ring Truss Structure

CHANGHYEON IM[1], WONGU SEO[2], CHANGSEONG KIM[2], SEULGI PARK[2], AND HOSUNG CHOO[1], (Senior Member, IEEE)
[1]Department of Electronic and Electrical Engineering, Hongik University, Seoul 04066, South Korea
[2]Hanwha Systems Company Ltd., Seongnam 13524, South Korea

Corresponding author: Hosung Choo (hschoo@hongik.ac.kr)

This work was supported by Korea Research Institute for Defense Technology Planning and Advancement (KRIT) grant funded by the Defense Acquisition Program Administration (DAPA), Korea Blue Force Tracking (BFT) Communication Satellite Large Antenna Technology, under Grant 21-307-A00-013.

ABSTRACT In this paper, we propose the optimal shape of a 1.5 m offset mesh reflector antenna using a deployable ring truss structure. The proposed antenna consists of a deployable mesh reflector and a feed antenna. The mesh reflectors are typically expanded by tension to maintain their parabolic structure; thus, shape deformation cannot be avoided compared to an ideal parabolic shape. To analyze the performance degradation caused by multiple flat subdivisions of the mesh, the bore-sight gain and main lobe direction are evaluated depending on the number of subdivisions. Additionally, their variations in accordance with the feed antenna's position and direction are analyzed in relation to the asymmetric structure of the offset reflector. To verify the performance of the mesh reflector antenna, a steel use stainless (SUS) mesh reflector (Prototype I), molybdenum mesh reflector (Prototype II), and the feed antenna are fabricated and measured in both near-field and far-field conditions. The measured bore-sight gains of Prototype I are 21.8 dBi (2 GHz), 23.9 dBi (3 GHz), 25.8 dBi (4 GHz), which agree well with the simulation results of 21.0 dBi, 24.1 dBi, and 26.4 dBi, respectively. In the case of Prototype II, the average bore-sight gain is approximately 3.7 dB lower than the simulation results. This is attributed to the displacement of the feed antenna caused by the gravitational sagging of the boom. In contrast to Prototype I, Prototype II mounts the feed antenna at the tip of the boom, making it more susceptible to deformation. To address this issue, a gravity-compensated (0G) measurement setup is planned for future studies.

INDEX TERMS Satellite antenna, deployable reflector antenna, mesh reflector, offset reflector.

I. INTRODUCTION

With significant advancements in satellite technology, the scope of satellite missions continues to expand to include communications, signal intelligence (SIGINT) collection, and Earth observation [1], [2], [3], [4], [5], [6], [7]. These missions require the collection of signals from ground-based stations and terrestrial sources. To enable this signal exchange between satellites and the Earth's surface, extremely high-gain antennas are required to compensate for significant path loss caused by long-distance transmission under atmospheric losses [8], [9], [10]. In addition, satellite antennas should have broadband characteristics to support various missions with a limited number of antennas. One of the antenna types that offers both high-gain and broadband characteristics is the reflector antenna, which is widely used in satellite missions [11], [12], [13]. Reflector antennas can achieve high-gain characteristics by increasing the diameter of the reflector, and their operating frequency is determined by the feed antenna. However, using a reflector antenna at high altitudes, such as geostationary Earth orbit (GEO), requires increasing its size to achieve high-gain characteristics. This increase in size results in the greater overall volume and weight of the antenna system, which

The associate editor coordinating the review of this manuscript and approving it for publication was Bilal A. Khawaja.

are critical drawbacks for rocket launch operations due to the limitations related to payload capacity. Therefore, it is crucial to minimize these disadvantages when applying a large-diameter reflector antenna to a satellite. To address this issue, various studies have been conducted on deployable mesh reflector antennas, which significantly reduce the stowed volume through the deployable structure and decrease weight by replacing the heavy solid reflectors with lightweight conducting mesh [14], [15], [16], [17], [18], [19], [20]. As the mesh cannot retain a defined shape on its own, it is supported by structural elements such as ribs and tension ties. These supporting structures generate tension to maintain the defined shape of the mesh surface, which in turn divides it into multiple flat subdivisions, thereby degrading the antenna's performance. In particular, ring truss reflector antennas often adopt an offset feeding method in which the feed antenna is positioned outside the reflector's aperture to reduce the blockage effect. As a result, to achieve high aperture efficiency, it is necessary to employ an asymmetrical reflector surface, unlike the symmetric design typically used in front-fed reflector antennas. Therefore, both the number and placement of the tension ties should be optimized, considering the asymmetrical structure of the reflector. Although many previous studies have been conducted on the design of mesh reflector antennas, most have remained at the theoretical level, with few cases involving actual fabrication and measurement for performance validation. In addition, many previous studies have focused on mechanical aspects, such as selecting the optimal structural configuration for deployability [21], [22], or improving the surface accuracy of the reflector [16], [23]. Therefore, it is necessary to analyze and optimize the performance of reflector antennas through simulation and to validate their performance by fabrication and measurements.

In this paper, we propose an optimal shape of a 1.5 m offset mesh reflector antenna using a deployable ring truss structure. The proposed antenna consists of a deployable mesh reflector and a feed antenna. The mesh reflectors are typically expanded by tension to maintain their parabolic structure; thus, shape deformation cannot be avoided compared to an ideal parabolic shape. To analyze the performance degradation caused by multiple flat subdivisions of the mesh, the bore-sight gain and main lobe direction are evaluated depending on the number of subdivisions. Additionally, their variations in accordance with the feed antenna's position and direction are analyzed, considering the asymmetric structure of the offset reflector. The performance of the mesh reflector is investigated using the CST Studio Suite full EM simulator [24]. Since the diameter of the mesh wire is very small (0.0023λ at 3 GHz) compared to the reflector diameter (15λ at 3 GHz), the total simulation time increases significantly [25]. To reduce the simulation time and computing resources, in the simulation, the mesh surface of the reflector is replaced by an ELCS that has the same reflectivity as the conducting mesh [14]. To verify the performance of the mesh reflector antenna, a steel use stainless (SUS) mesh reflector (Prototype I), a molybdenum mesh reflector (Prototype II), and the feed antenna are fabricated. Prototype I is fabricated to verify the reliability of the simulation, using SUS mesh with 10 openings per inch (OPI) as the reflective surface, which has a reflectivity of 61% at 3 GHz. In this prototype, the truss ring structure is fabricated using plastic 3D printing and is a fixed, non-deployable structure. In contrast, Prototype II is designed to be deployable and uses molybdenum mesh with 10 OPI as the reflective surface, which has a reflectivity of 90% at 3 GHz. The radiation patterns and bore-sight gains are then measured under both near-field and far-field conditions. The measured bore-sight gains of Prototype I are 21.8 dBi (2 GHz), 23.9 dBi (3 GHz), and 25.8 dBi (4 GHz), which agree well with the simulation results of 21.0 dBi, 24.1 dBi, and 26.4 dBi, respectively. In the case of Prototype II, the average bore-sight gain is approximately 3.7 dB lower than the simulation results. Through this fabrication and validation process, the proposed antenna has been verified and confirmed to be suitable for satellite applications. In terms of antenna performance, the proposed mesh reflector antenna has a drawback in aperture efficiency compared to a solid reflector antenna due to deformation of the reflective surface shape. However, it offers deployability and low weight, which allow it to be easily integrated into a rocket payload and reduce the launch costs.

II. GEOMETRY AND DESIGN METHOD OF THE PROPOSED ANTENNA

Fig. 1 illustrates the geometry of the deployable offset mesh reflector antenna. The proposed reflector antenna consists of a deployable mesh reflector and a feed antenna, as illustrated in Fig. 1(a). In general, a reflector redirects radio waves radiated from the feed antenna toward the bore-sight direction, achieving high-gain characteristics when the radio waves are reflected in parallel. To satisfy this condition, the reflector should have a parabolic shape optimized for the feed antenna distance (d_f). In the proposed reflector antenna, the feed antenna is placed outside the reflector's aperture to reduce the blockage effect. In this configuration, an asymmetrical reflector surface is required to ensure that the radio waves are reflected in parallel. Fig. 1(b) depicts a side view of the proposed antenna. The mesh reflector consists of a ring truss, a conducting mesh, a front cable net, and a rear cable net. The ring truss is deployable, which results in a reduced stowed volume when storing the reflector inside the payload. The conducting mesh, made of fiber material, is attached to the ring truss and unfolds when the truss is deployed. To serve as a substitute for a solid reflector and to effectively reflect radio waves, the mesh is typically designed to have a reflectivity of greater than 97%. In this study, a mesh with 97% reflectivity is applied in the simulation. The front and rear cable nets are used to maintain the shape of the mesh. The front cable net, located on the upper surface of the mesh, and the rear cable net, attached to the back rim of the ring truss, are connected by tension ties, as illustrated in Fig. 1(c). These tension ties generate tension to maintain the defined

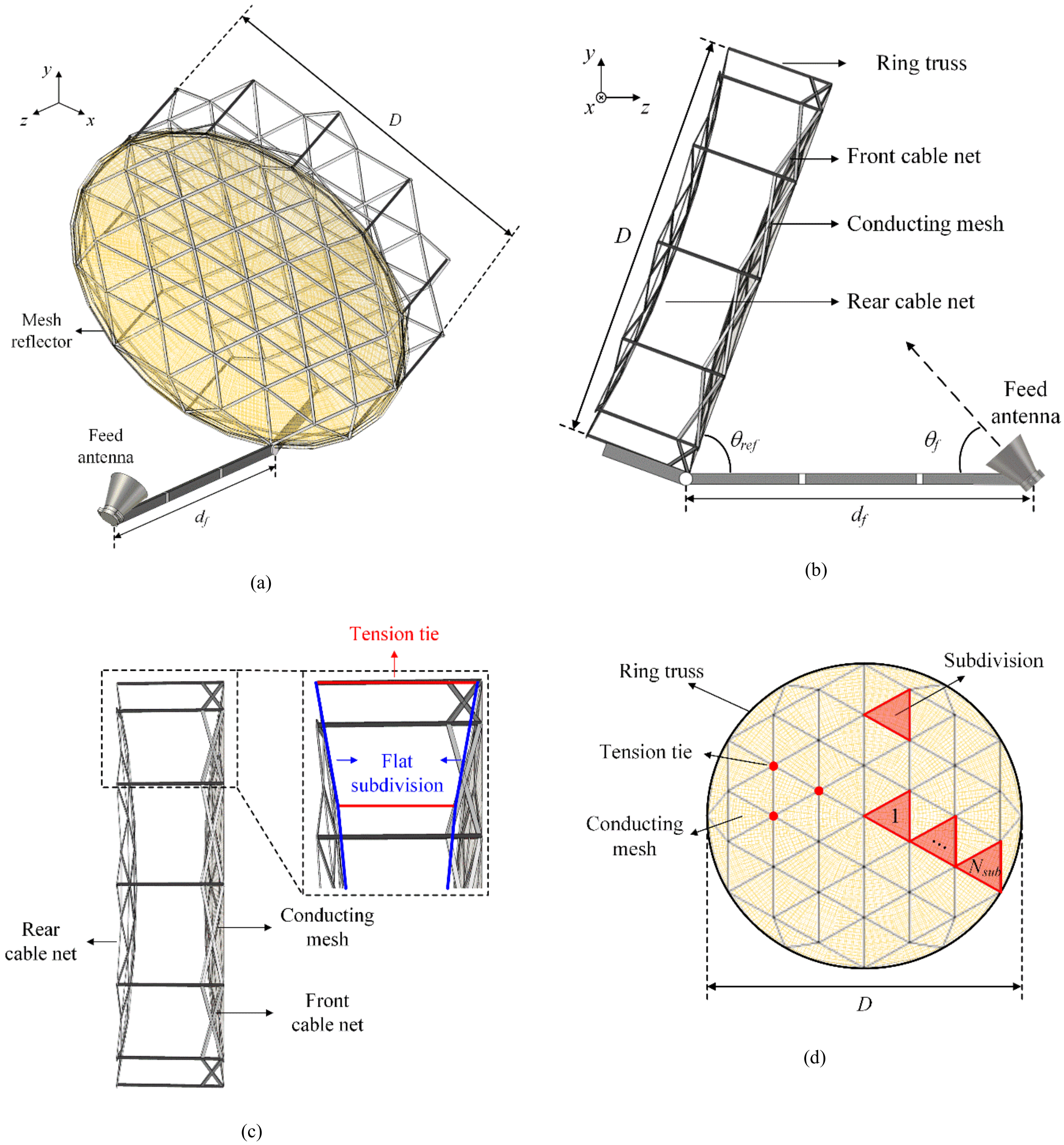

FIGURE 1. Geometry of the deployable mesh reflector antenna. (a) Isometric view. (b) Side view. (c) Side view of the reflector. (d) Front view of the reflector.

shape of the mesh surface, which in turn divides the mesh into multiple flat subdivisions. Fig. 1(d) presents a front view of the reflector, which shows the mesh surface divided into multiple flat subdivisions. Each subdivision has a flat reflective surface, which results in shape deformation and degradation in antenna performance compared to the ideal parabolic shape. Therefore, it is necessary to optimize the antenna performance with respect to the number of subdivisions (N_{sub}), reflector aperture angle (θ_{ref}), feed antenna distance (d_f), and feed antenna angle (θ_f). Fig. 2 shows the calculation process for the depth of mesh surface (d_m) used to determine the height of the truss structure. The deployed and stowed shapes have a same height, and the height of stowed shape defines the stowed volume. Therefore, minimizing this value is important for reducing the overall volume. The height of the truss structure is determined by the depth of mesh surface. To obtain the depth of mesh surface, we calculated the value using the following equation (1).

$$d_m = \frac{|z_u y_c - y_u z_c|}{\sqrt{z_u^2 + y_u^2}}$$
$$z_u = -2d_f + \sqrt{\left(2d_f\right)^2 + D^2}$$
$$y_u = \sqrt{-8d_f + 4d_f\sqrt{\left(2d_f\right)^2 + D^2}}$$
$$z_c = d_f\left(\frac{z_u}{y_u}\right)^2$$
$$y_c = 2d_f\frac{z_u}{y_u} \tag{1}$$

Here, d_m is the shortest distance obtained using the distance equation between a point and a line. y_u and z_u denote an upper edge point of offset mesh reflector, while y_c and z_c represent the tangent point between a mesh surface and a line having the same slope as the line connecting the origin (0, 0) and (y_u, z_u). To optimize the performance of the reflector antenna, it is analyzed using the CST Studio Suite full EM simulator. The detail parameters are then optimized and listed in Table 1.

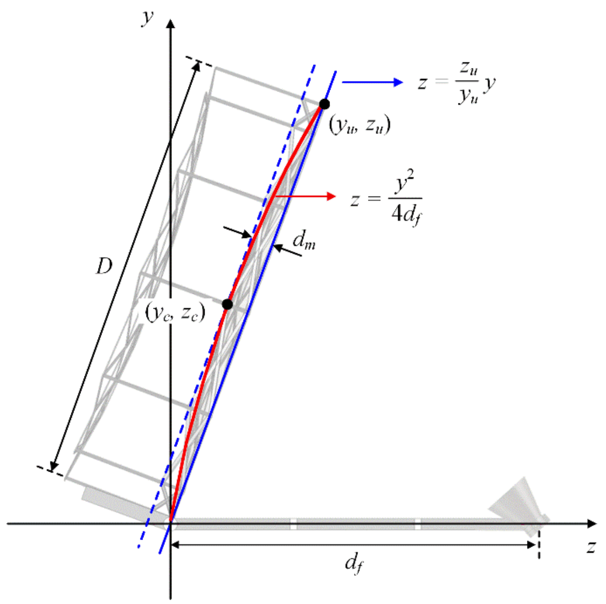

FIGURE 2. Calculation process for the depth of the mesh surface.

TABLE 1. Design parameters of the proposed antenna.

Parameters	Values
D	1.5 m
d_f	1.48 m
θ_{ref}	13.68°
θ_f	29°
d_m	0.086 m
N_{sub}	3

Fig. 3 indicates the design method of an offset reflector using the parabola equation. Reflectors are generally designed based on the parabola equation to reflect the radio waves radiated from the feed antenna parallel to the bore-sight or to concentrate the radio waves incident on the reflector toward the feed antenna [14], [26]. The proposed mesh reflector consists of multiple flat subdivisions on the reflector surface due to the tension tie; thus, it is important to model this on the parabolic surface. To design this surface in the simulation, we use the following equation (2), as presented in Fig. 2(a).

$$z_p = \frac{x_p^2 + y_p^2}{4 \times f} \tag{2}$$

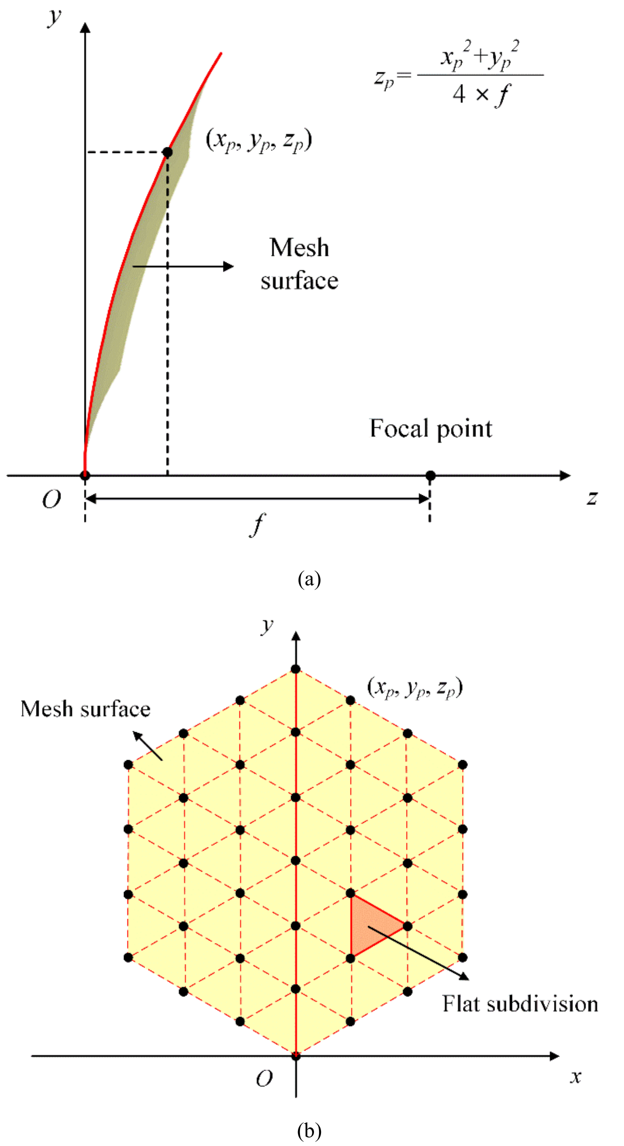

FIGURE 3. Design method of an offset reflector using the parabola equation in the simulation. (a) Side view. (b) Front view.

Here, x_p, y_p, and z_p denote the coordinates of the tension tie connection point on the parabolic surface, and f represents the focal point. By connecting three adjacent points, a flat triangular subdivision is modeled, as illustrated in Fig. 2(b). Fig. 4 presents a simulation setup for the mesh surface using an effective lossy conducting surface (ELCS). Since the diameter of the mesh wire is very small (0.0023λ at 3 GHz) compared to the reflector diameter (15λ at 3 GHz), the total simulation time increases significantly. To reduce the simulation time and computing resources, in the simulation, the mesh surface of the reflector is replaced by an ELCS that has the same reflectivity as the conducting mesh [13]. In this study, we use two types of mesh, namely steel use stainless (SUS) mesh and molybdenum mesh. The SUS mesh with 10 openings per inch (OPI) has a reflectivity of 61% at 3 GHz, and molybdenum mesh with 10 OPI has a reflectivity of 90%

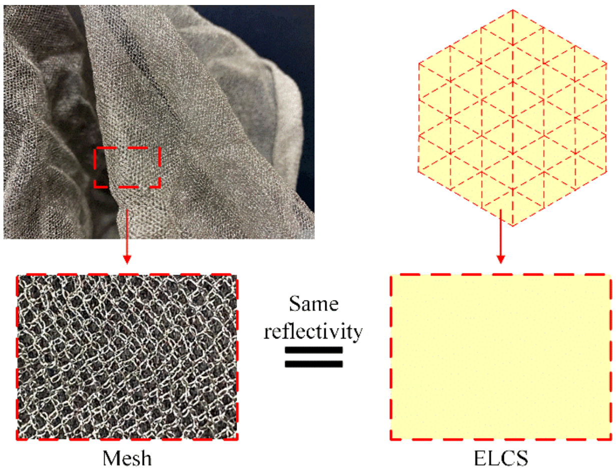

FIGURE 4. Simulation setup for the mesh surface using an ELCS.

at 3 GHz, respectively. To achieve the same reflectivity for each mesh, the conductivities of the ELCS are determined in accordance with frequency.

III. ANALYSIS OF DESIGN PARAMETERS

Fig. 5 illustrates bore-sight gain and half power beam width (HPBW) in accordance with the number of subdivisions (N_{sub}). As shown here, when the number of subdivisions increases, the shape is complicated. Thus, it is important to determine the appropriate number of subdivisions. For this, we analyze the reflector antenna performance, such as bore-sight gain and HPBW, according to the number of subdivisions. When N_{sub} is greater than 3, both characteristics remain constant at each frequency without further increases or decreases. Therefore, three subdivisions are applied to the proposed reflector. Fig. 6 indicates the main lobe direction and bore-sight gain in accordance with the angle of the reflector (θ_{ref}). When the angle of the reflector changes, the change in the bore-sight gain remains relatively stable, while the direction of the main lobe changes significantly. In practical operations, it is difficult to adjust the angle of the reflector according to the frequency, so a specific angle should be determined that does not move significantly from 0° at all frequencies. When the angle is 13.68°, the main lobe direction appears as 0.06° at 2 GHz, −0.06° at 3 GHz, and −0.01° at 4 GHz, respectively.

Fig. 7 demonstrates bore-sight gain in accordance with the feed antenna distance (d_f) and angle (θ_f). Figs. 6(a), 6(b), and 6(c) illustrate the bore-sight gain at 2 GHz, 3 GHz, and 4 GHz. As shown in these figures, the optimal parameters that yield maximum gain differ at each frequency. However, it is difficult to adjust the distance and angle of the feed antenna for each operating frequency. Therefore, to determine the point of minimal gain reduction across all frequencies, we calculate the average gain reduction based on the maximum gain points at each frequency, as shown in Fig. 6(d). When d_f and θ_f are set to 1.48 m and 29°, respectively, the average gain degradation is −0.077 dB.

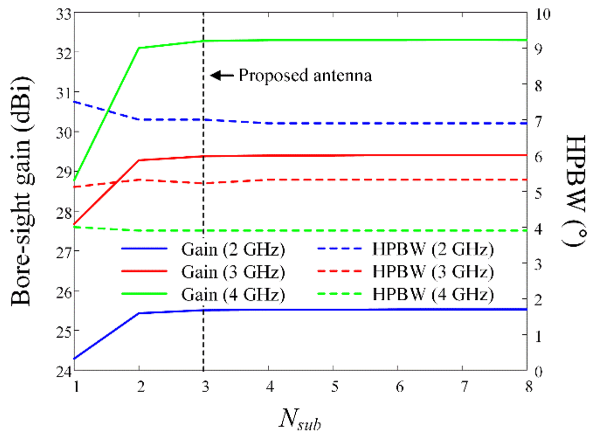

FIGURE 5. Bore-sight gain and HPBW in accordance with N_{sub}.

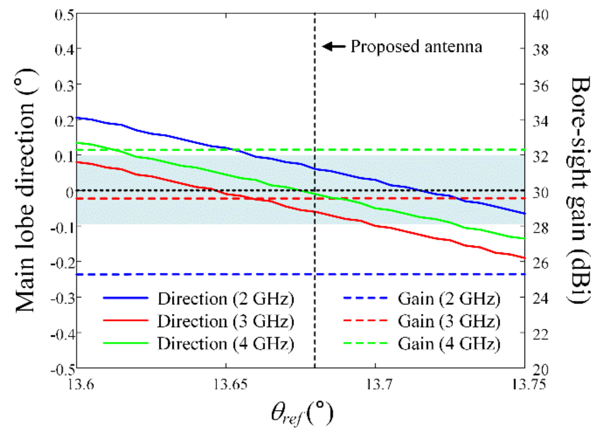

FIGURE 6. Main lobe direction and bore-sight gain in accordance with θ_{ref}.

IV. FABRICATION AND MEASUREMENT

Fig. 8 illustrates photographs of the fabricated reflector antenna (Prototype I). Prototype I is fabricated to verify the reliability of the simulation, using the SUS mesh with 10 openings per inch (OPI) as the reflective surface, which has a reflectivity of 61% at 3 GHz. In this prototype, the truss ring structure is fabricated using plastic 3D printing and is a fixed, non-deployable structure. Fig. 8(a) shows the fabricated mesh reflector, which consists of the SUS mesh, plastic truss structure, and tension ties. To maintain the defined shape of the mesh surface, polyester strings are used as tension ties. This reflector is then mounted on a Styrofoam jig (ε_r =1.03, $\tan\delta = 0.0001$) along with the feed antenna for measurement, as shown in Fig. 8(b). Fig. 9 shows the reflection coefficients of the proposed antenna, where solid and dashed lines indicate the measured and simulated results, respectively. The measured reflection coefficient shows broadband of less than −10 dB from 2 GHz to 4 GHz, which agrees well with the simulation results.

Fig. 10 presents photographs of the near-field measurement setup and the radiation pattern results of Prototype I. To verify the performance of the proposed antenna, the

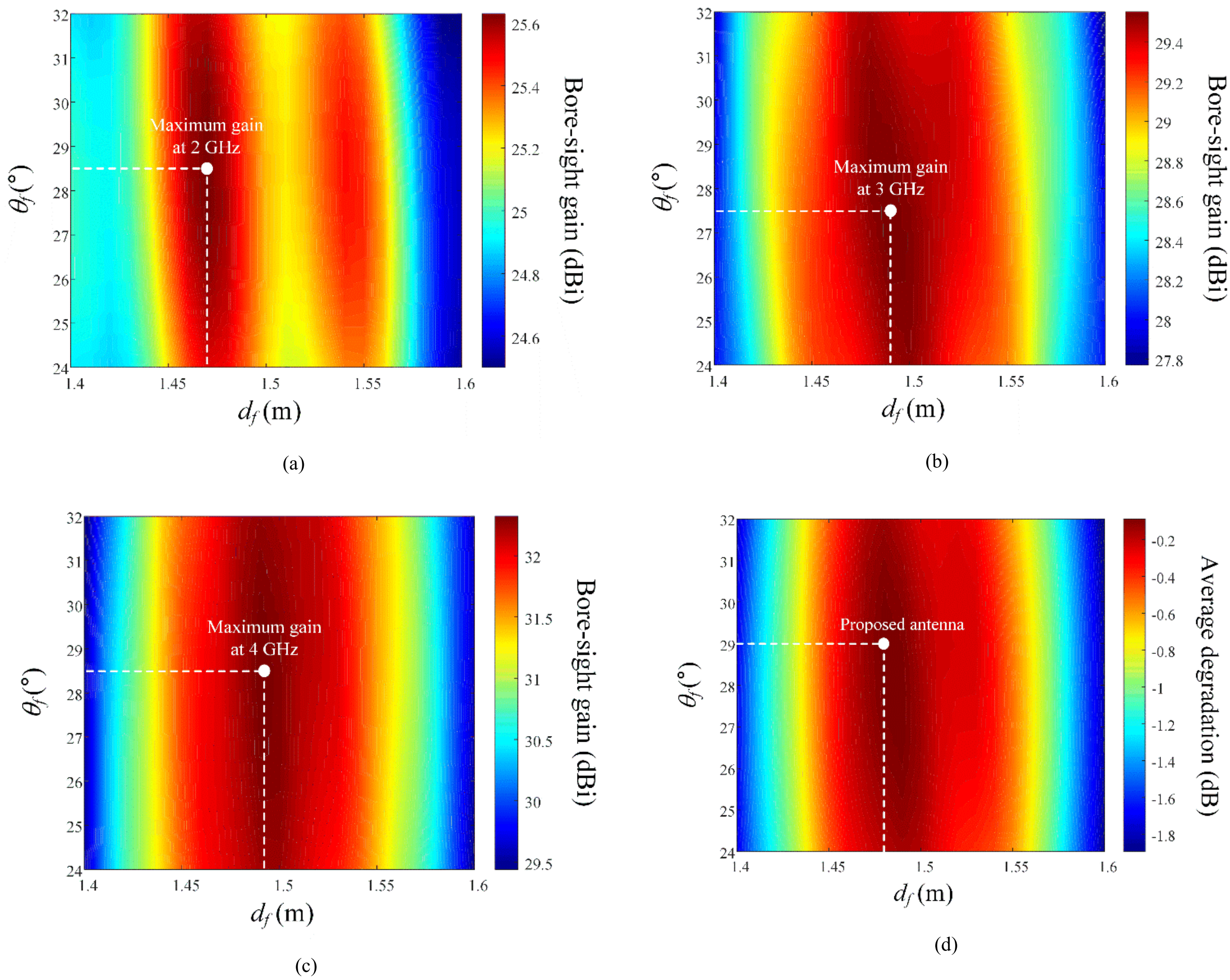

FIGURE 7. Bore-sight gain in accordance with d_f and θ_f. (a) 2 GHz. (b) 3 GHz. (c) 4 GHz. (d) Average degradation.

near-field measurements are taken, as shown in Fig. 10(a). The scan area is 2 m by 2 m, which is the maximum range of a scanner. The measured near-field results are then transformed into the radiation patterns using the near-field to far-field (NF2FF) algorithm [27]. Fig. 10(b), 10(c), and 10(d) show the radiation patterns of the proposed antenna, where the solid and dashed lines indicate the measured and simulated results, respectively. At 2 GHz in the φ =0° plane, the measured bore-sight gain and HPBW are 21.8 dBi and 7.0°, which agree well with the simulated results of 21.0 dBi and 6.7°. In the φ =90° plane, the measured bore-sight gain and HPBW are 21.8 dBi and 5.5°, which agree well with the simulated results of 21.0 dBi and 6.7°. Fig. 11 shows the measurement setup and results of the proposed antenna in the far-field environment. To ensure far-field conditions, the reflector antenna and the probe antenna are aligned face-to-face at a distance of 120 m (in far-field region). In this setup, a signal generator is connected to the reflector's feeder antenna to supply transmitted power, and a spectrum analyzer is connected to the probe antenna to measure the received power. The bore-sight gain of the proposed antenna (G_r) is then calculated using the Friis equation with the measured transmitted and received power, as indicated in equations (3) and (4).

$$G_r = P_r - P_r - L_p - L_s - G_p \tag{3}$$

$$L_p = 20\log_{10}\left(\frac{\lambda}{4\pi d}\right) \tag{4}$$

where P_r denotes received power measured by the spectrum analyzer, and P_t represents transmitted power supplied to the feeder antenna from the signal generator. L_p and L_s refer to the path loss and system loss, respectively, which includes losses from RF cables, connectors, the signal generator, and the spectrum analyzer. Since these two losses must be compensated for when calculating the antenna gain, L_p and L_s are typically negative values. G_p indicates the bore-sight gain of the probe antenna. Fig. 11(b) illustrates the bore-sight gain of the proposed antenna, where the '×' markers and dashed lines represent the measured and simulated results, respectively. From 2 GHz to 4 GHz, the measured results agree

TABLE 2. Comparisons between the proposed antenna and previous studies.

Research	Dia.	Electrical analysis	Bore-sight gain	Aperture Effi.	Fab. / Meas.
[14]	1 m	O	31.6 dBi @ 10 GHz	13.2% @ 10 GHz	O / O
[15]	6 m	X	-	-	O / X
[17]	2.5 m	O	36.84 dB @ 3 GHz (directivity)	29.6% @ 3 GHz	X / X
[23]	2.5 m	X	-	-	O / X
This work	1.5 m	O	29.5 dBi @ 3 GHz	40% @ 3 GHz	O / O

well with the simulated results, with an average difference of 1.11 dB.

Fig. 12 presents photographs of the measurement setup in an anechoic chamber and radiation pattern results of Prototype II. The fabricated reflector antenna consists of a mesh reflector, boom, and feed antenna. This antenna is designed to be deployable and uses a molybdenum mesh with 10 OPI as the reflective surface, which has a reflectivity of 90% at 3 GHz. To measure the radiation patterns in an anechoic chamber, the antenna is mounted on a rotator that can rotate in both φ and θ directions, as illustrated in Fig. 12(a). At 2 GHz, the measured bore-sight gain is 20.7 dBi with a main lobe direction of 2°, which represents a 3.8 dB decrease and a 2° tilt compared with the simulated results. At other frequencies, the measured results are 4.5 dB lower at 3 GHz and 2.9 dB lower at 4 GHz, respectively. These differences are attributed to the displacement of the feed antenna caused by the gravitational sagging of the boom. In contrast to Prototype I, Prototype II mounts the feed antenna at the tip of the boom, making it more susceptible to deformation. Although additional structures could be attached to fix the boom position and eliminate errors, the fabricated Prototype II antenna is designed with the same configuration as the final operational antenna for satellite integration, to evaluate its electrical and mechanical performance. To address this issue, a gravity-compensated (0G) measurement setup is planned for future studies. Table 2 shows the comparisons between the proposed antenna and previous studies. The studies [15] and [23] proposed designs for deployable mesh antennas. Although the proposed antennas demonstrated deployability and were fabricated, the studies focused on mechanical analysis without electrical analysis. In contrast, studies [14] and [17] included electrical analyses. The antenna proposed in [14], a deployable rib-type mesh reflector, was analyzed

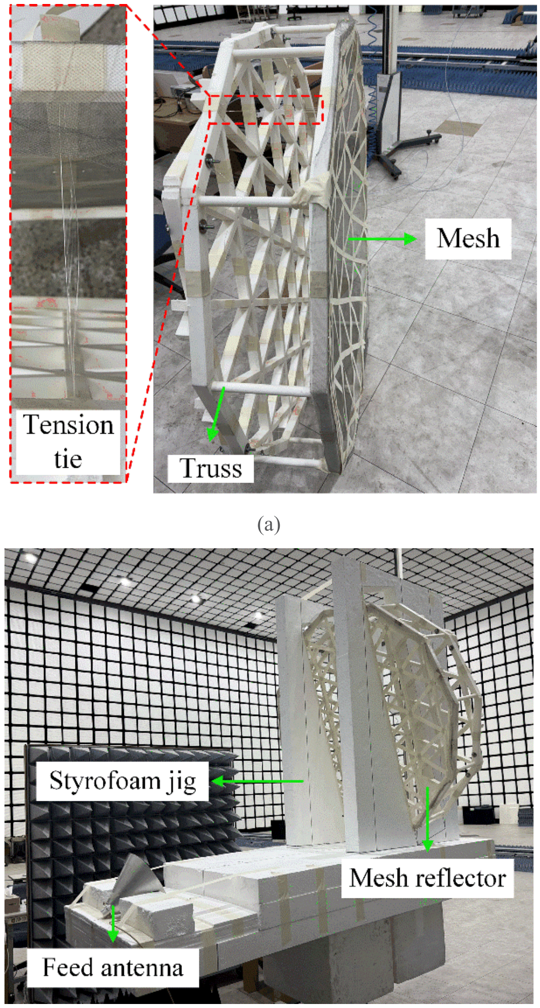

FIGURE 8. Photographs of the fabricated reflector antenna (Prototype I). (a) Mesh reflector. (b) Mesh reflector with a feed antenna.

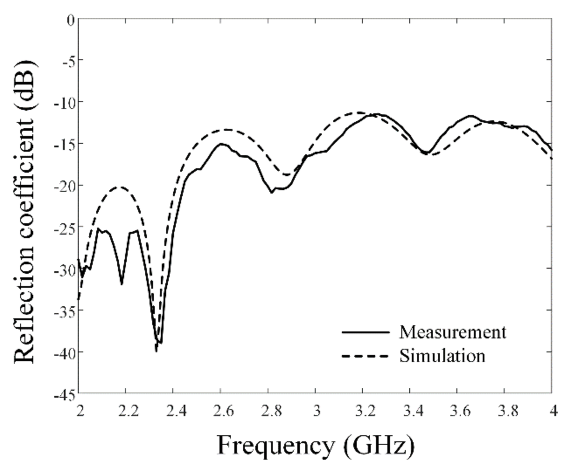

FIGURE 9. Measured and simulated reflection coefficients of the proposed antenna.

from an electrical perspective and subsequently fabricated and measured; however, its aperture efficiency was only

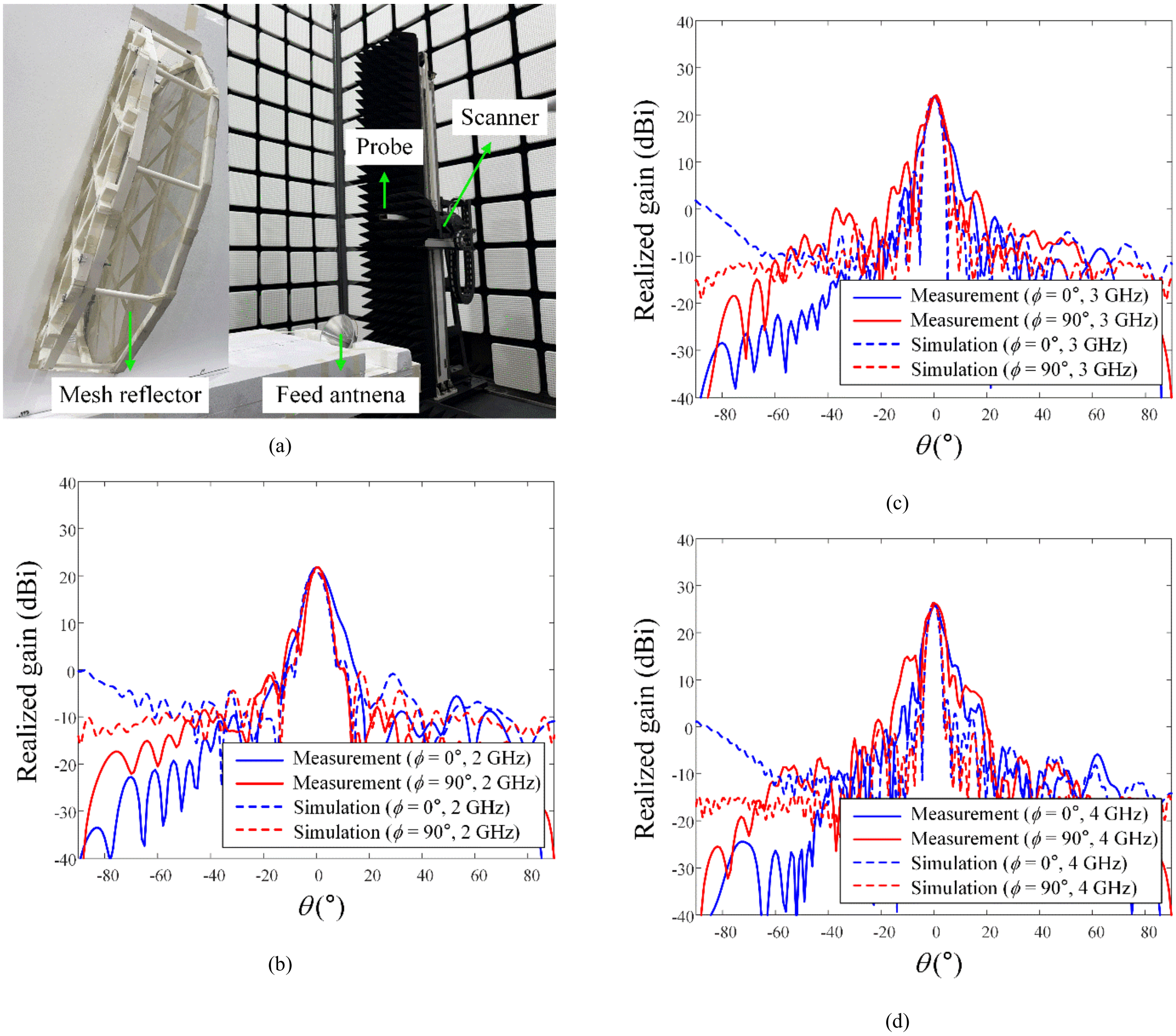

FIGURE 10. Photographs of the near-field measurement setup and radiation patterns of Prototype I. (a) Measurement setup. (b) 2 GHz. (c) 3 GHz. (d) 4 GHz.

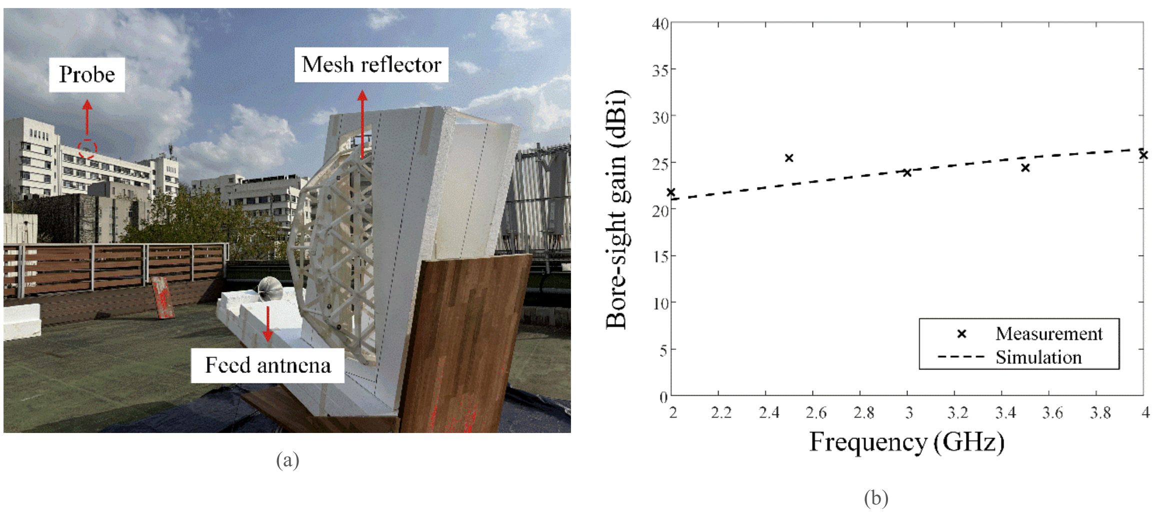

FIGURE 11. Photographs of the near-field measurement setup and bore-sight gain results of Prototype I. (a) Measurement setup. (b) Bore-sight gain.

13.2% at 10 GHz. The design proposed in [17] achieved a higher aperture efficiency of 29.6% at 3 GHz; this value is still lower than ours, and the antenna was not fabricated to verify feasibility. The results demonstrate the suitability of

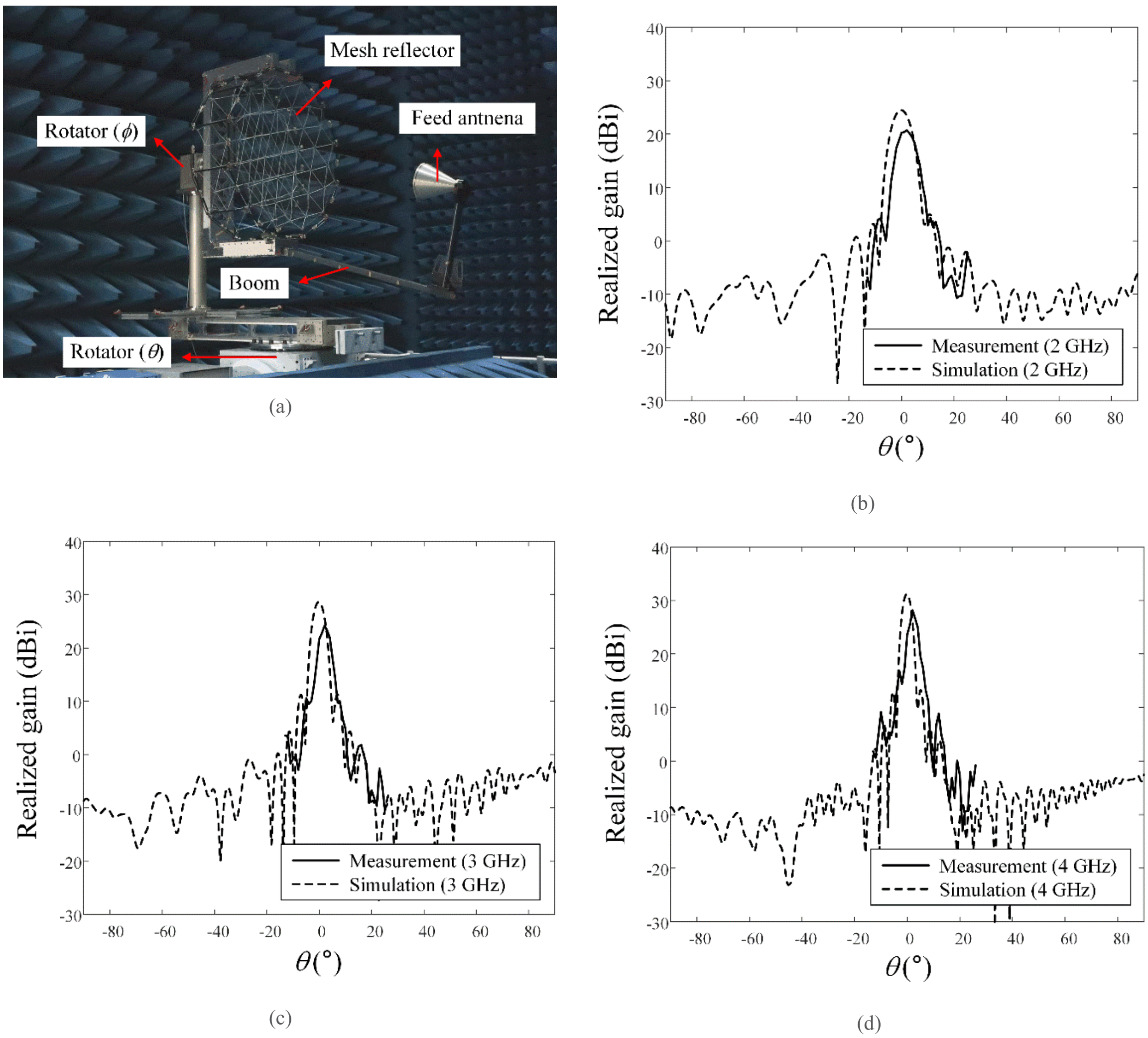

FIGURE 12. **Photographs of the measurement setup in an anechoic chamber and radiation pattern results of Prototype II. (a) Measurement setup. (b) 2 GHz. (c) 3 GHz. (d) 4 GHz.**

the proposed deployable offset mesh reflector antenna for satellite applications, achieving an aperture efficiency of 40% at 3 GHz, with feasibility verified through fabrication and measurement.

V. CONCLUSION

In this paper, we proposed the optimal shape of a 1.5 m offset mesh reflector antenna using a deployable ring truss structure. The proposed antenna consisted of a deployable mesh reflector and a feed antenna. The mesh reflectors were typically expanded by tension to maintain their parabolic structure; thus, shape deformation could not be avoided compared to an ideal parabolic shape. To analyze the performance degradation caused by multiple flat subdivisions of the mesh, the bore-sight gain and main lobe direction were evaluated depending on the number of subdivisions. Additionally, their variations in accordance with the feed antenna's position and direction were analyzed, considering the asymmetric structure of the offset reflector. To verify the performance of the mesh reflector antenna, a steel use stainless (SUS) mesh reflector (Prototype I), a molybdenum mesh reflector (Prototype II), and the feed antenna were fabricated and measured in both near-field and far-field conditions. The measured bore-sight gains of Prototype I were 21.8 dBi (2 GHz), 23.9 dBi (3 GHz), and 25.8 dBi (4 GHz), which agreed well with the simulation results of 21.0 dBi, 24.1 dBi, and 26.4 dBi, respectively. In the case of Prototype II, the average bore-sight gain was approximately 3.7 dB lower than the simulation results. This was attributed to the displacement of the feed antenna caused by the gravitational sagging of the boom. In contrast to Prototype I, Prototype II mounted the feed antenna at the tip of the boom, making it more susceptible to deformation. To address this issue, a gravity-compensated (0G) measurement setup is planned for future studies.

REFERENCES

[1] O. Kodheli, E. Lagunas, N. Maturo, S. K. Sharma, B. Shankar, J. F. M. Montoya, J. C. M. Duncan, D. Spano, S. Chatzinotas, S. Kisseleff, J. Querol, L. Lei, T. X. Vu, and G. Goussetis, "Satellite communications in the new space era: A survey and future challenges," *IEEE Commun. Surveys Tuts.*, vol. 23, no. 1, pp. 70–109, 1st Quart., 2021.

[2] F. Fourati and M.-S. Alouini, "Artificial intelligence for satellite communication: A review," *Intell. Converged Netw.*, vol. 2, no. 3, pp. 213–243, Sep. 2021.

[3] P.-Y. Le Traon et al., "Use of satellite observations for operational oceanography: Recent achievements and future prospects," *J. Oper. Oceanogr.*, vol. 8, no. sup1, pp. s12–s27, Apr. 2015.

[4] S.-P. Xie, "Satellite observations of cool ocean–atmosphere interaction," *Bull. Amer. Meteorolog. Soc.*, vol. 85, no. 2, pp. 195–208, Feb. 2004.

[5] S. J. Goetz, A. Baccini, N. T. Laporte, T. Johns, W. Walker, J. Kellndorfer, R. A. Houghton, and M. Sun, "Mapping and monitoring carbon stocks with satellite observations: A comparison of methods," *Carbon Balance Manage.*, vol. 4, no. 1, pp. 1–7, Dec. 2009.

[6] S.-J. Kim, S. J. Maeng, J.-H. Lim, J. W. Lee, T.-K. Lee, and W. K. Lee, "Performance evaluation of spaceborne bistatic SAR systems," *J. Electromagn. Eng. Sci.*, vol. 24, no. 3, pp. 318–326, May 2024.

[7] B.-H. Shim, Y.-J. Yu, and K.-M. Song, "Survey on advances in broadband signal generation and processing of ASIC semiconductors for defense satellites," *J. Electromagn. Eng. Sci.*, vol. 24, no. 4, pp. 377–383, Jul. 2024.

[8] A. Al-Hourani and I. Guvenc, "On modeling satellite-to-ground path-loss in urban environments," *IEEE Commun. Lett.*, vol. 25, no. 3, pp. 696–700, Mar. 2021.

[9] O. Ahmadien, H. F. Ates, T. Baykas, and B. K. Gunturk, "Predicting path loss distribution of an area from satellite images using deep learning," *IEEE Access*, vol. 8, pp. 64982–64991, 2020.

[10] H. F. Ates, S. M. Hashir, T. Baykas, and B. K. Gunturk, "Path loss exponent and shadowing factor prediction from satellite images using deep learning," *IEEE Access*, vol. 7, pp. 101366–101375, 2019.

[11] R. C. Gupta, S. K. Sagi, K. P. Raja, N. K. Sharma, and R. Jyoti, "Shaped prime-focus reflector antenna for satellite communication," *IEEE Antennas Wireless Propag. Lett.*, vol. 16, pp. 1945–1948, 2017.

[12] E. G. Geterud, J. Yang, T. Ostling, and P. Bergmark, "Design and optimization of a compact wideband hat-fed reflector antenna for satellite communications," *IEEE Trans. Antennas Propag.*, vol. 61, no. 1, pp. 125–133, Jan. 2013.

[13] F. Greco, L. Boccia, E. Arnieri, and G. Amendola, "K/Ka-band cylindrical reflector antenna for compact satellite Earth terminals," *IEEE Trans. Antennas Propag.*, vol. 67, no. 8, pp. 5662–5667, Aug. 2019.

[14] C. Im, W. Seo, S. Park, K. Kim, S. Park, and H. Choo, "Design of a deployable broadband mesh reflector antenna for a SIGINT satellite system considering surface shape deformation," *Sensors*, vol. 24, no. 2, p. 384, Jan. 2024.

[15] J.-S. Choi, T.-Y. Park, B.-G. Chae, and H.-U. Oh, "Development of lightweight 6 m deployable mesh reflector antenna mechanisms based on a superelastic shape memory alloy," *Aerospace*, vol. 11, no. 9, p. 738, Sep. 2024.

[16] Z. Liu, M. Zhu, D. Yang, C. Zhang, and Y. Liu, "An overall form-finding method of cable-membrane-truss for super-large mesh reflectors considering large-deformation trusses," *Thin-Walled Struct.*, vol. 215, Oct. 2025, Art. no. 113536.

[17] J. Zhang, B. He, R. Nie, G. Wang, L. Zhang, and Y. Fan, "Beamforming design of a mesh reflector antenna with novel structural configurations," *IEEE Trans. Antennas Propag.*, vol. 73, no. 8, pp. 5770–5777, Aug. 2025.

[18] L.-Y.-O. Yang, H.-Y. Lin, and B. Tsai, "Gain enhancement and sidelobe suppression of an X-band dual-polarized deployable mesh reflector antenna using a symmetrical, angle-insensitive reflective metasurface," *IEICE Commun. Exp.*, vol. 14, no. 1, pp. 12–16, Jan. 2025.

[19] J. Zhang, B. He, R. Nie, G. Wang, and Y. Fan, "Anti-creep pretension determination of a mesh reflector antenna for long term surface accuracy retention," *Comput. Struct.*, vol. 301, Sep. 2024, Art. no. 107460.

[20] S.-A. Lee, S.-J. Jo, S.-J. Kim, T.-K. Lee, and J. W. Lee, "Analysis of cross-polarized field by panel misalignment errors in a deployable reflector antenna," *J. Electromagn. Eng. Sci.*, vol. 23, no. 1, pp. 18–26, Jan. 2023.

[21] O. Sushko, E. Medzmariashvili, L. Filipenko, A. Tsiklauri, G. Medzmariashvili, M. Nikoladze, S. Tserodze, D. Vasylenko, O. Shpylka, S. Khoroshylov, S. Martyniuk, and V. Vasyliev, "Modified design of the deployable mesh reflector antenna for mini satellites," *CEAS Space J.*, vol. 13, no. 4, pp. 533–542, Oct. 2021.

[22] P. Yuan, B. He, L. Zhang, H. Jiang, R. Nie, and X. Ma, "Topology generation and optimization of boundary cable nets for the mesh reflector antenna," *Eng. Struct.*, vol. 229, Feb. 2021, Art. no. 111630.

[23] R. Zhang, Y. Zhang, H. Guan, N. Hu, and J. Lai, "Efficient and high-precision adjustment of mesh reflector antenna considering target consistency," *Space, Sci. Technol.*, vol. 5, pp. 1–19, Jan. 2025.

[24] *CST Studio Suite: Electromagnetic Field Simulation Software*. Accessed: Jul. 5, 2019. [Online]. Available: http://www.cst.com

[25] J. Huang, Y. Yoo, S.-J. Jo, C.-W. Seo, S.-A. Lee, S.-S. Yoon, and S.-O. Park, "Analysis of the characteristics of mesh with complex knitting patterns for spaceborne reflector antennas," *J. Electromagn. Eng. Sci.*, vol. 24, no. 6, pp. 565–573, Nov. 2024.

[26] S. K. Rao, "Parametric design and analysis of multiple-beam reflector antennas for satellite communications," *IEEE Antennas Propag. Mag.*, vol. 45, no. 4, pp. 26–34, Aug. 2003.

[27] A. Balanis, *Antenna Theory*. Hoboken, NJ, USA: Wiley, 2016.

CHANGHYEON IM received the B.S. degree in electronic and electrical engineering from Hongik University, Seoul, South Korea, in 2021, where he is currently pursuing the Ph.D. degree in electronic and electrical engineering. His research interests include mesh reflector antenna, 5G application, wireless power transfer, and ultra-wideband antenna.

WONGU SEO received the B.S. and M.S. degrees in electrical engineering from Chungnam National University, in 2014 and 2016, respectively. Since January 2016, he has been with the Tactical Communication System Team, Hanwha Systems. His major research fields include satellite antennas, electronic warfare systems, and tactical communication systems.

CHANGSEONG KIM received the B.S. and integrated M.S./Ph.D. degrees from the Department of Electrical and Computer Engineering, Ajou University, Suwon, South Korea, in 2015 and 2021, respectively. Since 2021, he has been a Researcher with Hanwha Systems, Pangyo, South Korea. His research interests include the tropospheric wave propagation, array antenna, and reflector antenna.

SEULGI PARK received the B.S. and M.S. degrees in electrical engineering from Hongik University, in 2006 and 2008, respectively. He was with the Electronic Warfare Research Center, LIG Nex1 Corporation, from 2008 to 2013. From 2013 to 2016, he was with the DMC Research Center, Samsung Electronics Corporation. Since January 2017, he has been with the Tactical Communication System Team, Hanwha Systems. His major research fields include electronic warfare transmission/reception antennas, electronic warfare systems, and tactical communication systems.

HOSUNG CHOO (Senior Member, IEEE) received the B.S. degree in radio science and engineering from Hanyang University, Seoul, South Korea, in 1998, and the M.S. and Ph.D. degrees in electrical and computer engineering from the University of Texas at Austin, in 2000 and 2003, respectively. In September 2003, he joined the School of Electronic and Electrical Engineering, Hongik University, Seoul, where he is currently a Professor. His principal areas of research include electrically small antennas for wireless communications, reader and tag antenna for RFID, on-glass and conformal antennas for vehicles and aircraft, and array antenna for GPS applications.

• • •